Antisense oligonucleotides target a nearly invariant structural element from the SARS-CoV-2 genome and drive RNA degradation

(Valeria Lulla[1], Michal P. Wandel[2], Katarzyna J. Bandyra[3], Tom Dendooven[3], Xiaofei Yang[4])*, Nicole Doyle[5], Stephanie Oerum[6], Sara O'Rourke[7], Felix Randow[2], Helena J. Maier[5], [William Scott[7], Yiliang Ding[4], Andrew E. Firth[1], Kotryna Bloznelyte[3], Ben F. Luisi[3]]**

*These joint-first authors made complementary and equivalent contributions
**To whom correspondence may be addressed

[1]Department of Pathology, Division of Virology, University of Cambridge, Lab Block Level 5, Addenbrookes Hospital, Hills Road, Cambridge CB2 0QQ, U.K.

[2]MRC Laboratory of Molecular Biology, Francis Crick Avenue, Cambridge, CB2 0QH, U.K.

[3]Department of Biochemistry, University of Cambridge, Tennis Court Road, Cambridge CB2 1GA, U.K.

[4]Department of Cell and Developmental Biology, John Innes Centre, Norwich Research Park, Norwich, NR4 7UH, U.K.

[5]Pirbright Institute, Ash Road, Pirbright, Woking, GU24 ONF, U.K.

[6]CNRS-Université Paris Diderot, Institut de Biologie Physico-Chimique, 13 rue Pierre et Marie Curie, 75005 Paris, France

[7]University of California at Santa Cruz, Santa Cruz California, 95064, U.S.A.

Summary:
The SARS-CoV-2 virus contains an unusually large, single-stranded RNA genome that is punctuated with structured elements of unknown function, such as the s2m element located in the 3′ untranslated region. The evolutionary conservation of the s2m element and its occurrence in all viral subgenomic transcripts implicates a key role in the viral infection cycle. In order to exploit this element as a potential therapeutic target, we have designed antisense "gapmer" oligonucleotides that efficiently base-pair to the s2m region. These oligonucleotides, composed of locked nucleic acids (LNA) flanking a central DNA core, successfully remodel the s2m structure and induce sequence-specific RNA cleavage by RNase H *in vitro*. Gapmers are also effective in human cells as they reduce the fluorescence signal in GFP reporter assays and cause a dose-dependent reduction in replication in a model replicon system based on a human astrovirus. Overall, these oligonucleotides show promise as anti-viral agents and may serve as a helpful starting point to develop treatments for COVID-19.

Keywords: SARS-CoV-2, COVID-19, therapeutic oligonucleotides, gapmer, positive-sense RNA virus, coronavirus, astrovirus, LNA

INTRODUCTION

SARS-CoV-2 is a highly infectious virus and the causative agent of the ongoing COVID-19 pandemic. Given the continued rise in cases worldwide, the significant mortality rate and the challenges in predicting the severity of illness in infected individuals (Messner et al., 2020), there is a pressing need for efficacious antiviral therapies. This is currently not addressed by infection prevention, as there is a lack of available vaccines and uncertainty as to whether any developed ones will provide long-lasting immunity (Koirala et al., 2020; https://www.who.int/emergencies/diseases/novel-coronavirus-2019). Moreover, the potential for further outbreaks of infections by other coronaviruses (Akula and McCubrey, 2020) places importance on exploring therapeutic avenues in order to build capability for handling potential situations beyond the current COVID-19 health crisis.

Like other positive-sense (+) single-stranded (ss) RNA viruses, replication of SARS-CoV-2 is orchestrated by virus-encoded enzymes inside infected host cells. The 30 kb long SARS-CoV-2 genomic RNA and the subgenomic mRNA transcripts all contain a common 5′-leader sequence and a common 3′ UTR, which harbour several conserved structural elements, including the stem-loop 2 motif (s2m) (Fig. 1A and B) (Rangan et al., 2020; Kim et al., 2020). The s2m, originally identified in astroviruses (Jonassen et al., 1998), is a highly conserved RNA sequence element, present within the 3′ UTR in the genomes of many astroviruses, some picornaviruses and noroviruses, and a variety of coronaviruses, including members of the subgenus *Sarbecovirus*, which includes the SARS-CoV and SARS-CoV-2 viruses (Tengs et al., 2013, Tengs et al., 2016). The s2m sequences of 41 nucleotides (nt) are nearly identical between SARS-CoV and SARS-CoV-2, with just 2 nt differences within the elements, greatly contrasting the overall 20 % genome-wide sequence difference (Kim et al., 2020). Importantly, the s2m sequence is consistently present among the clinical isolates from patients that have tested positive for SARS-CoV-2 during the current pandemic (GSAID database https://www.gisaid.org; UCSC genome browser). The high degree of s2m sequence conservation is likely to be a direct consequence of a requirement to sustain an elaborate and conserved three-dimensional structure. Indeed, an earlier study of the SARS-CoV s2m element revealed a stem loop with exposed bases (Fig. 1B) in a 2.7 Å resolution crystal structure (Robertson et al., 2005). Experimental mapping of RNA-RNA interactions of the positive sense SARS-CoV-2 viral species, probed within the host cell, is consistent with the s2m element being structured, and possibly pairing with open reading frame ORF1a at some stage (Ziv et al., 2020).

Because of the apparent high degree of selective pressure to maintain this specific sequence and its structure, the s2m is a promising target for potential antiviral agents, with low likelihood of evolving mutations that would lead to resistance. Any agents targeting the s2m element would also have the advantage of acting against a large number of viral RNA species, due to the presence of the element in all positive-sense viral RNAs, including both the genomic and the subgenomic mRNAs.

Antisense oligonucleotides (ASOs) may offer one means of targeting specific viral genomic elements such as the s2m. These oligonucleotides have proven therapeutic potential against viruses and have been undergoing active development for more than a decade. Third generation ASOs include locked nucleic acids (LNAs), in which a bicyclic linkage at the furanose constrains the conformational freedom of the nucleotide (Singh et al., 1998). The LNA provides high affinity base-pairing to complementary RNA and DNA targets, as well as

resistance to nuclease attack (Hagedorn et al., 2018). A version of LNA ASOs known as 'gapmers' consists of LNA bases flanking a central DNA sequence. In this design, LNA bases confer resistance to nucleases and provide high-affinity base-pairing to target RNA. The central DNA region, once base-paired to RNA, recruits ribonuclease H (RNase H), which acts to cleave the RNA in the RNA-DNA duplex. In this process, the DNA is not digested and thus the gapmer remains intact and free to bind further RNA molecules. Gapmers have already been successfully used in clinical trials to silence target transcripts (Bonneau et al., 2019).

In this report, we describe the design and testing of several LNA-based gapmers against the SARS-CoV-2 virus. In particular, we focused ASO design on the highly conserved structured s2m element that resides in the 3′ UTR of all plus-sense viral RNA species, including genomic RNA and subgenomic mRNAs. We found that the LNA-based gapmers successfully disrupt s2m structure and induce sequence-specific RNA cleavage *in vitro*. Gapmers also proved to be effective in human cells, reducing expression of GFP reporter genes that carry the SARS-CoV-2 s2m element in their 3′ UTR and causing a dose-dependent reduction in virus replication in model replicon assays. These and other gapmers may be suitable lead compounds for further development as antiviral therapeutics to treat COVID-19 and illnesses caused by related viruses.

RESULTS

Model for the s2m element in the context of the SARS-CoV-2 3′ UTR

The SARS-CoV s2m RNA crystal structure at 2.7Å resolution (Robertson et al., 2005) revealed a stem loop with a small pocket that accommodates cations (Fig. 1B). The sequence similarity of the SARS-CoV and SARS-CoV-2 s2m elements (Fig. 1A) indicates structural similarity. We confirmed the predicted structure of the s2m element within the 3′ UTR of the SARS-CoV-2 RNA using RNA structure probing by SHAPE (**S**elective 2′-**H**ydroxyl **A**cylation analyzed by **P**rimer **E**xtension) (Spitale et al., 2013) with the reagent 2-methylnicotinic acid imidazolide (NAI). The signals of SHAPE-induced reverse-transcription stalling were identified by polyacrylamide gel electrophoresis (PAGE) (Fig. 1C), and further used to generate SHAPE reactivity values for each nucleotide, with a high value indicative of a single-stranded nature. The SHAPE reactivity profile strongly agrees with the crystal structure of the SARS-CoV s2m element. For instance, high SHAPE reactivities were found at the loop region (G71-A75), indicating strong possibility of a single-stranded nature, while low SHAPE reactivities were found on nucleotides predicted to be base-paired, such as nucleotides from 54 to 58, and nucleotides from 90 to 94. We further performed SHAPE probing on an extended version of the 3' UTR RNA (extended 3′ UTR) that additionally includes ORF10 and the region immediately upstream from it (ORF10 may not be protein coding; Taiaroa et al., 2020; Jungreis et al., 2020) (Fig. 1A and S1 and Table 1). We found a high degree of consistency between the SHAPE profiles for the s2m element in the extended and non-extended version (Pearson correlation coefficient PCC = 0.996, Fig. S1B and S1C), indicating that the s2m element in the 3′ UTR is stably folded and is unlikely to be affected by flanking regions such as ORF10.

To further investigate potential structures formed by the 3′ UTR and the extended 3′ UTR that includes ORF10, we used cryo-electron microscopy. Analysis of these RNAs mainly indicated elongated shapes resembling thick rope (Fig. 1D). The ropey particles are up to 500 Å in length, although a subset of particles are more compact, at 300 Å, as observed after 2D/3D

averaging approaches (Fig. 1E and F). The latter is about half the length expected for an elongated polymer, implying that the RNA is semi-compact, but without apparent conformational definition at the global level. The shapes are consistent with features observed from tomography of cells infected with SARS-CoV-2 virus (Klein et al., 2020). Both in the *in situ* tomograms and in our single-particle cryo-EM images there were unidentified small, high-contrast features observed at the periphery of the RNA particles (Fig. 1D, red arrows). It is likely that these dots represent views along the long axis of duplex regions.

In conclusion, our structure probing results, along with the structural prediction from the SARS-CoV s2m RNA crystal structure, confirm that the s2m element in the 3′ UTR of SARS-CoV-2 RNA folds into a stem-loop structure, which may be highly conserved among coronaviruses.

Design of LNA gapmers against the s2m element; assessment of binding and activity *in vitro*

The highly conserved nature of the s2m element makes it an attractive target for therapies based on antisense oligonucleotides (ASOs), including the high-affinity, nuclease-resistant LNA gapmers. However, the structured nature of the target may – on the other hand – interfere with ASO-target base-pairing. To overcome this, and to facilitate gapmer-induced disruption of the native s2m structure, we directed the high-affinity LNA bases to pair with the bases predicted to be exposed in the s2m element (Fig. 2 and Table 3). This pairing should facilitate initial gapmer-target interaction and could then lead to unfolding of the s2m element as the rest of the gapmer base-pairs with the complementary target nucleotides.

We first tested the ability of the gapmers to direct RNase H cleavage *in vitro*, using s2m RNA as the substrate for the purified enzyme (Fig. 2A and D). Gapmers 1-3 were designed to have higher affinity for target RNA than gapmers 4-6, as indicated by respective predicted melting temperatures (schematic top panel, Fig. 2 and Table 3). The presence of sequence-specific gapmers 1-6 in the reaction led to clear degradation of target RNA, whereas non-sequence-specific control gapmer with scrambled sequence failed to have an effect ("scr", Fig. 2D). The degradation was very efficient even for 2:1 s2m:gapmer molar ratio, indicating that gapmers can be recycled and direct multiple turnover of substrates by RNase H. Gapmers also drove cleavage of the 3′ UTR (Fig. 2B and E) and the extended 3′ UTR that includes ORF10 and the region immediately upstream of it (Fig. 2F), indicating that the target s2m sequence is successfully recognised and is accessible for gapmer base-pairing in its native sequence context. The observation that both the higher-affinity gapmers 1-3 (Fig. 2A and B) and the lower-affinity gapmers 4-6 (Fig. 2 D, E and F) were able to direct RNase H cleavage of the s2m element indicates that a range of gapmer-target affinities are compatible with successful target degradation of the highly structured s2m sequence.

We also designed and tested gapmers targeting one of the conserved regions predicted to be single-stranded in the SARS-CoV-2, at positions 1359-1374 relative to the NC_045512.2 viral reference genome ("ss3"; Rangan et al., 2020). In the presence of RNase H, these gapmers, named "all" and "some", caused efficient target degradation *in vitro* (Fig. 2C), indicating general applicability of gapmer-induced degradation of viral RNA sequences. Gapmers "all" and "some" have the same sequence and base composition, but different polymer backbones (Table 3). The entire backbone of gapmer "all" contains phosphorothioate modifications, as is also the case in gapmers 1-6; it is a well-established modification conferring some nuclease resistance to oligonucleotides (Kumar et al., 1998; Eckstein, 2000). The backbone in gapmer

"some", however, is mixed; DNA bases are linked by phosphodiester backbone, whereas LNA bases are linked by phosphorothioate backbone. Our in vitro digestion experiments (Fig. 2C) indicate that both chemistries are compatible with RNase H recruitment and target degradation. Gapmer "some" appears to have higher affinity for the "ss3" RNA target element, judging from the presence of the extra band at the top of the gel in Fig. 2C; this is consistent with expectation, as phosphorothioate modifications are known to reduce target affinity (Grünweller et al., 2003). Meanwhile, gapmer "all" generates a higher amount of cleaved product, which supports our choice of phosphorothioate backbone throughout gapmers 1-6.

LNA gapmers remodel the s2m structure

To test whether the gapmers disrupt the s2m structure, we repeated the SHAPE probing of 3′UTR of SARS-CoV-2 in the presence of these ASOs (gapmers 1, 2 and 3 targeting s2m and gapmer 'all' as a non-specific control). Since SHAPE probing detects the accessibility of nucleotides (Spitale et al., 2013), it is also capable of revealing intra- and inter-molecular RNA base-pairing interactions. To ensure stable s2m folding, the RNA was denatured and refolded, then gapmers were added and incubated together with the RNA, followed by NAI probing (see Methods).

In the presence of gapmer 1 and gapmer 2, SHAPE reactivity profiles strongly decreased at the regions targeted by the gapmers, indicating inter-molecular interactions formed between gapmers and their target sequences (Fig. 3A-D). In contrast, SHAPE reactivities strongly increased in the regions that were originally base-paired with the gapmer-target regions and in their flanking regions, indicating these regions were more single-stranded in the presence of gapmers.

In the presence of gapmer 3, which targets the single-stranded loop region within s2m, SHAPE reactivity profile showed a strong decrease in this region (Fig. 3E and F), indicating successful targeting by gapmer. We also found that this inter-molecular interaction between gapmer 3 and the loop region led to increased SHAPE reactivities downstream of the loop region. Thus, the inter-molecular interactions between gapmers and target regions could also remodel the folding status of flanking regions.

Notably, the SHAPE reactivity change is dependent on the concentration of gapmers and is not observed in the presence of a control gapmer (gapmer "all") which is not able to target the s2m element (Fig. 3G and H). Taken together, our results validate the design of gapmers in targeting the s2m element in the SARS-CoV-2 RNA, and highlight the effect of gapmers in remodelling s2m structure.

LNA gapmers against s2m effectively silence gene expression in a fluorescence reporter assay in human cells

To investigate if the s2m element influences RNA translation in human cells, we created a tissue culture-based assay. We generated HeLa and lung-derived A549 reporter cell lines carrying stably integrated GFP genes that encode either the wild type s2m element or a scrambled control sequence in the 3′ UTR (Fig. S2A and B). No difference was observed in the fluorescence levels between the GFP-s2m and GFP-scrambled cells, indicating that the s2m element does not affect the levels of fluorescent protein produced (Fig. S2C). This suggests that the s2m element, by itself, does not affect gene expression *in cis* for the s2m-containing viral mRNAs.

Next, we investigated if gapmers against the s2m element could drive target RNA silencing in human cells using the established HeLa and A549 cell lines with the stably integrated GFP-s2m reporter. Transfection with gapmers against s2m reduced GFP fluorescence levels in the two cell lines for both the higher-affinity gapmers 1-3 and the lower-affinity gapmers 5-6 (Fig. 4A and B). Gapmer 4, the shortest of the tested gapmers and containing only six DNA nucleotides (Table 3), had no effect (Fig. 4A and B); this may reflect difficulties in recruiting human RNase H *in vivo* to this length of RNA-DNA duplex (Kurreck et al., 2002). Non-specific control gapmers did not affect GFP fluorescence levels, nor did treatment with s2m-specific gapmers of control cell lines in which the sequence of the s2m element was scrambled (Fig. S3A and B). These results indicate that the silencing effect relies on sequence-specific gapmer-target interaction. Overall, the results show that gapmers against the s2m element have the potential to silence gene expression from mRNAs containing s2m in their 3′ UTR sequences, which is the case for SARS-CoV-2 mRNAs.

LNA gapmers inhibit replication in an astrovirus replicon model system in human cells

Many (+)ssRNA viruses share a similar repertoire of genetic elements required for the replication of viral RNA. Despite large differences in genome size, coronaviruses and astroviruses possess a similar modular organization, including the order of non-structural and structural genes, a frameshift signal to access the RNA-dependent RNA polymerase (RdRp) open reading frame, and production of 3′-coterminal subgenomic mRNAs for structural and accessory protein expression. Like coronaviruses, many astroviruses – including human astrovirus 1 (HAstV1) – also contain an s2m element in the 3′ UTR of their genomes (Fig. 5A). We have recently developed a robust HAstV1-based replicon system (Fig. 5A, lower panel), which allows us to evaluate RNA replication in different cell types (Lulla and Firth, 2020). The small genome size (~7 kb) of this model system, compared to coronaviruses (~30 kb), allows for much more rapid manipulation.

Using the astrovirus system, we tested the gapmers in the context of virus-like replication where, for example, viral replicative intermediates are generally occluded within host membrane derived vesicles, as is also the case in viral infection. First, we generated chimeric astrovirus replicons bearing the s2m elements from SARS-CoV or SARS-CoV-2 (Fig. 5B). The resulting chimeric replicons recapitulated the replication properties of the wild-type astrovirus replicon (Fig. 5C), confirming that this system is suitable for testing gapmers against SARS-CoV-2 s2m. To guard against potential cell-specific effects, all gapmers were tested in two human cell lines – Huh7.5.1 (Lulla and Firth, 2020) and HEK293T (optimised for this study). The replication of replicons bearing SARS-CoV-2 s2m sequences was efficiently inhibited by gapmers 1, 2, and 5 causing inhibition in the sub-nanomolar range, with a less pronounced effect found for gapmers 3, 4, and 6. The inhibition of non-specific control gapmers (“all” and “scr”) was significantly below their sequence-specific counterparts, gapmers 1-3 and 4-6, respectively (Fig. 5D). The same gapmers were also tested against the SARS-CoV s2m in this system and found to be active, though with a lower potency (Fig. 5E). This could potentially be attributed to differences arising from C-G versus C-U base pairing within the s2m elements (Fig. 5B), thus affecting the s2m structure and gapmer binding properties. Replication in the presence of sufficient concentrations of gapmers 1, 2 or 5 dropped to the baseline level of the pO2RL-GNN mutant, which is completely deficient in replication due to a mutated RdRp active site (Fig. 5C).

To assess the cytotoxicity and potential off-target effects of the tested gapmers, we (i) performed a lactate dehydrogenase (LDH) release-based cytotoxicity assay, and (ii) evaluated the efficiency of cap-dependent translation in the presence of the different gapmer concentrations. Consistent with previous work (Kaur et al., 2007), these assays showed no gapmer-induced cellular toxicity (Fig. S4A). Translation inhibition of > 50% was only observed at 500 nM concentrations of gapmers 1, 2, 5 and 6 (Fig. S4B), which is at least 10-fold higher than the effective inhibition range for gapmers 1, 2 and 5. Overall, these results suggest that gapmers targeting the s2m element can inhibit viral replication in the model replicon system without causing significant cell toxicity.

DISCUSSION

We have identified the highly conserved structural s2m element in the 3′ UTR of SARS-CoV-2 RNA as a feasible candidate for ASO-based anti-viral therapies. We designed LNA-based gapmers against the s2m element and tested these in multiple assays *in vitro* and *in vivo*. We demonstrated gapmer-induced disruption of the RNA structure consistent with successful gapmer-target base-pairing interactions, and RNase H-induced target degradation *in vitro*. We further demonstrated gapmer-induced sequence-specific silencing of target gene expression in GFP reporter assays in human cells. To test the ability of the gapmers to inhibit viral replication, we used an astrovirus-based replicon model system and developed a rapid functional assay not requiring access to higher containment level facilities. These viral replicon assays showed that gapmers against s2m inhibit viral replication in a sequence-specific, dose-dependent manner, down to sub-nanomolar range. These observations confirm that gapmers have significant potential as RNA replication inhibitors and should be tested in SARS-CoV-2 infected cells and developed animal models. Preliminary results indicate that gapmers may not be so effective against SARS-CoV-2 in human cell cultures at 100 nM, and further work may be required to optimise delivery.

It is worth noting that coronaviruses produce double membrane vesicles inside infected host cells, thought to conceal the viral double-stranded RNA replicative intermediate from cellular defences (Hagemeijer et al., 2012; Knoops et al., 2008). These vesicles have been proposed to be formed through virus-induced manipulations of the ER membrane (Blanchard and Roingeard, 2015). This compartmentalization of the SARS-CoV-2 genome in membranous bodies within the host cell's cytoplasm (Klein et al., 2020) may limit access of the ASOs to the s2m element or other viral genomic targets and impair the recruitment of endogenous RNase H. In this regard, it is useful to consider that LNA ASOs have been conjugated with tocopherol and cholesterol for membrane association in the past (Benizri et al., 2019; Nishina et al., 2015), which could be helpful to improve the efficacy of the gapmers against coronaviruses inside host cells. Improved membrane association may also boost gapmer entry into target cells. The action of gapmers may also benefit from combination therapeutics with other antiviral compounds, such as RNA polymerase inhibitors, achieving optimal efficacy and further dampening the potential emergence of resistance. The primary target cells for the SARS-CoV-2 infection are the ciliated airway cells of the respiratory tract (Hou et al., 2020), which could be amenable to aerosol delivery of the gapmers and other therapeutic compounds.

The results presented here represent a promising start for further research and development of gapmers and related ASOs targeting the s2m element in SARS-CoV-2. Gapmer designs may need further improvements for efficacy in cell culture and animal models, which could be

achieved through large scale optimisation and screening, as well as modifications for optimal delivery to target cells.

ACKNOWLEDGEMENTS

KJB, TD, KB and BFL are supported by a Wellcome Trust Investigator Award (200873/Z/16/Z) and TD by an Astra-Zeneca Studentship. X.Y and Y.D. are supported by a European Commission Horizon 2020 European Research Council (ERC) Starting Grant (680324). AEF and VL are supported by Wellcome Trust (106207) and European Research Council (646891) grants to AEF. All cryoEM grids were prepared and cryoEM data collected at the BIOCEM facility, Department of Biochemistry, University of Cambridge. We thank Dr Dimitri Y. Chirgadze, Dr Steve Hardwick and Mr Lee Cooper for assistance with data collection at the CryoEM Facility. We thank Henrik Oerum, Alex Borodavka and Chris Oubridge for invaluable advice and helpful discussions. We thank Dingquan Yu and Zhichao Miao for help with sequence analysis. We thank the support staff in our institutions for their invaluable help throughout the pandemic lockdown period.

REFERENCES

Akula, S. M., & McCubrey, J. A. (2020). Where are we with understanding of COVID-19?. *Advances in biological regulation*, *77*, 100745. https://doi.org/10.1016/j.jbior.2020.100745

Bonneau, E., Neveu, B., Kostantin, E., Tsongalis, G. J., & De Guire, V. (2019). How close are miRNAs from clinical practice? A perspective on the diagnostic and therapeutic market. *EJIFCC*, *30*(2), 114–127.

Benizri, S., Gissot, A., Martin, A., Vialet, B., Grinstaff, M. W., & Barthélémy, P. (2019). Bioconjugated Oligonucleotides: Recent Developments and Therapeutic Applications. *Bioconjugate chemistry*, *30*(2), 366–383. https://doi.org/10.1021/acs.bioconjchem.8b00761

Blanchard, E., & Roingeard, P. (2015). Virus-induced double-membrane vesicles. *Cellular microbiology*, *17*(1), 45–50. https://doi.org/10.1111/cmi.12372

Eckstein F. (2000). Phosphorothioate oligodeoxynucleotides: what is their origin and what is unique about them?. *Antisense & nucleic acid drug development*, *10*(2), 117–121. https://doi.org/10.1089/oli.1.2000.10.117

Grünweller, A., Wyszko, E., Bieber, B., Jahnel, R., Erdmann, V. A., & Kurreck, J. (2003). Comparison of different antisense strategies in mammalian cells using locked nucleic acids, 2'-O-methyl RNA, phosphorothioates and small interfering RNA. *Nucleic acids research*, *31*(12), 3185–3193. https://doi.org/10.1093/nar/gkg409

Hagedorn, P. H., Persson, R., Funder, E. D., Albæk, N., Diemer, S. L., Hansen, D. J., Møller, M. R., Papargyri, N., Christiansen, H., Hansen, B. R., Hansen, H. F., Jensen, M. A., & Koch, T. (2018). Locked nucleic acid: modality, diversity, and drug discovery. *Drug discovery today*, *23*(1), 101–114. https://doi.org/10.1016/j.drudis.2017.09.018

Hagemeijer, M. C., Vonk, A. M., Monastyrska, I., Rottier, P. J., & de Haan, C. A. (2012). Visualizing coronavirus RNA synthesis in time by using click chemistry. *Journal of virology*, *86*(10), 5808–5816. https://doi.org/10.1128/JVI.07207-11

Hou, Y. J., Okuda, K., Edwards, C. E., Martinez, D. R., Asakura, T., Dinnon, K. H., 3rd, Kato, T., Lee, R. E., Yount, B. L., Mascenik, T. M., Chen, G., Olivier, K. N., Ghio, A., Tse, L. V., Leist, S. R., Gralinski, L. E., Schäfer, A., Dang, H., Gilmore, R., Nakano, S., … Baric, R. S. (2020). SARS-CoV-2 Reverse Genetics Reveals a Variable Infection Gradient in the Respiratory Tract. *Cell*, *182*(2), 429–446.e14. https://doi.org/10.1016/j.cell.2020.05.042

Jungreis, I., Sealfon, R., & Kellis, M. (2020). Sarbecovirus comparative genomics elucidates gene content of SARS-CoV-2 and functional impact of COVID-19 pandemic mutations. *bioRxiv : the preprint server for biology*, 2020.06.02.130955. https://doi.org/10.1101/2020.06.02.130955

Kaur, H., Babu, B. R., & Maiti, S. (2007). Perspectives on chemistry and therapeutic applications of Locked Nucleic Acid (LNA). *Chemical reviews, 107*(11)*,* 4672–4697. https://doi.org/10.1021/cr050266u

Kim, D., Lee, J. Y., Yang, J. S., Kim, J. W., Kim, V. N., & Chang, H. (2020). The Architecture of SARS-CoV-2 Transcriptome. *Cell*, *181*(4), 914–921.e10. https://doi.org/10.1016/j.cell.2020.04.011

Klein, S., Cortese, M., Winter, S.L., Wachsmuth-Melm, M., Neufeldt, C.J., Cerikan, B., Stanifer, M.L., Boulant, S., Bartensclager, R. and Chlanda, P. (2020) SARS-CoV-2 structure and replication characterised by in situ cryo-electron tomography. bioRxiv 2020.06.23.167064; doi: https://doi.org/10.1101/2020.06.23.167064

Knoops, K., Kikkert, M., Worm, S. H., Zevenhoven-Dobbe, J. C., van der Meer, Y., Koster, A. J., Mommaas, A. M., & Snijder, E. J. (2008). SARS-coronavirus replication is supported by a reticulovesicular network of modified endoplasmic reticulum. *PLoS biology*, *6*(9), e226. https://doi.org/10.1371/journal.pbio.0060226

Koirala, A., Joo, Y. J., Khatami, A., Chiu, C., & Britton, P. N. (2020). Vaccines for COVID-19: The current state of play. *Paediatric respiratory reviews*, S1526-0542(20)30095-6. Advance online publication. https://doi.org/10.1016/j.prrv.2020.06.010

Kumar, R., Singh, S. K., Koshkin, A. A., Rajwanshi, V. K., Meldgaard, M., & Wengel, J. (1998). The first analogues of LNA (locked nucleic acids): phosphorothioate-LNA and 2'-thio-LNA. *Bioorganic & medicinal chemistry letters*, *8*(16), 2219–2222. https://doi.org/10.1016/s0960-894x(98)00366-7

Kurreck, J., Wyszko, E., Gillen, C., & Erdmann, V. A. (2002). Design of antisense oligonucleotides stabilized by locked nucleic acids. *Nucleic acids research*, *30*(9), 1911–1918. https://doi.org/10.1093/nar/30.9.1911

Low, J. T., & Weeks, K. M. (2010). SHAPE-directed RNA secondary structure prediction. *Methods (San Diego, Calif.)*, *52*(2), 150–158. https://doi.org/10.1016/j.ymeth.2010.06.007

Lulla, V., & Firth, A. E. (2020). A hidden gene in astroviruses encodes a viroporin. *Nature communications*, *11*(1), 4070. https://doi.org/10.1038/s41467-020-17906-x

Messner, C. B., Demichev, V., Wendisch, D., Michalick, L., White, M., Freiwald, A., Textoris-Taube, K., Vernardis, S. I., Egger, A. S., Kreidl, M., Ludwig, D., Kilian, C., Agostini, F., Zelezniak, A., Thibeault, C., Pfeiffer, M., Hippenstiel, S., Hocke, A., von Kalle, C., Campbell, A., … Ralser, M. (2020). Ultra-High-Throughput Clinical Proteomics Reveals Classifiers of COVID-19 Infection. *Cell systems*, *11*(1), 11–24.e4. https://doi.org/10.1016/j.cels.2020.05.012

Nishina, T., Numata, J., Nishina, K., Yoshida-Tanaka, K., Nitta, K., Piao, W., Iwata, R., Ito, S., Kuwahara, H., Wada, T., Mizusawa, H., & Yokota, T. (2015). Chimeric Antisense Oligonucleotide Conjugated to α-Tocopherol. *Molecular therapy. Nucleic acids*, *4*(1), e220. https://doi.org/10.1038/mtna.2014.72

Punjani, A., Rubinstein, J. L., Fleet, D. J., & Brubaker, M. A. (2017). cryoSPARC: algorithms for rapid unsupervised cryo-EM structure determination. *Nature methods*, *14*(3), 290–296. https://doi.org/10.1038/nmeth.4169

Rangan, R., Zheludev, I. N., Hagey, R. J., Pham, E. A., Wayment-Steele, H. K., Glenn, J. S., & Das, R. (2020). RNA genome conservation and secondary structure in SARS-CoV-2 and SARS-related viruses: a first look. *RNA (New York, N.Y.)*, *26*(8), 937–959. https://doi.org/10.1261/rna.076141.120

Robertson, M. P., Igel, H., Baertsch, R., Haussler, D., Ares, M., Jr, & Scott, W. G. (2005). The structure of a rigorously conserved RNA element within the SARS virus genome. *PLoS biology*, *3*(1), e5. https://doi.org/10.1371/journal.pbio.0030005

Singh, S.K., Koshkin, A.A., Wengel, J. and Nielsen, P. (1998) LNA (locked nucleic acids): synthesis and high-affinity nucleic acid recognition. *Chem. Commun.* 4, 455–456. doi: 10.1039/A708608C

Spitale, R. C., Crisalli, P., Flynn, R. A., Torre, E. A., Kool, E. T., & Chang, H. Y. (2013). RNA SHAPE analysis in living cells. *Nature chemical biology*, *9*(1), 18–20. https://doi.org/10.1038/nchembio.1131

Taiaroa G et al. 2020. Direct RNA sequencing and early evolution of SARS-CoV-2. bioRxiv 2020.03.05.976167; doi: https://doi.org/10.1101/2020.03.05.976167

Tegunov, D., & Cramer, P. (2019). Real-time cryo-electron microscopy data preprocessing with Warp. *Nature methods*, *16*(11), 1146–1152. https://doi.org/10.1038/s41592-019-0580-y

Tengs, T., & Jonassen, C. M. (2016). Distribution and Evolutionary History of the Mobile Genetic Element s2m in Coronaviruses. *Diseases (Basel, Switzerland)*, *4*(3), 27. https://doi.org/10.3390/diseases4030027

Tengs, T., Kristoffersen, A. B., Bachvaroff, T. R., & Jonassen, C. M. (2013). A mobile genetic element with unknown function found in distantly related viruses. *Virology journal*, *10*, 132. https://doi.org/10.1186/1743-422X-10-132

Wang, C., Liu, Z., Chen, Z., Huang, X., Xu, M., He, T., & Zhang, Z. (2020). The establishment of reference sequence for SARS-CoV-2 and variation analysis. *Journal of medical virology*, *92*(6), 667–674. https://doi.org/10.1002/jmv.25762

Zhong, J., Gastaminza, P., Cheng, G., Kapadia, S., Kato, T., Burton, D. R., Wieland, S. F., Uprichard, S. L., Wakita, T., & Chisari, F. V. (2005). Robust hepatitis C virus infection in vitro. *Proceedings of the National Academy of Sciences of the United States of America*, *102*(26), 9294–9299. https://doi.org/10.1073/pnas.0503596102

Ziv O, Price J, Shalamova L, Kamenova T, Goodfellow I, Weber F, Miska E. 2020. The short and long-range RNA-RNA interactome of SARS-CoV-2. bioRxiv 2020.07.19.211110; doi: https://doi.org/10.1101/2020.07.19.211110

FIGURES

A

UUCAC CGAG GCC A CG CG GAGUA CG AU CG AG UGU ACA GUGAA SARS-CoV-2
UUCAU CGAG GCC A CG CG GAGUA CG AU CG AG GGU ACA GUGAA SARS-CoV

B

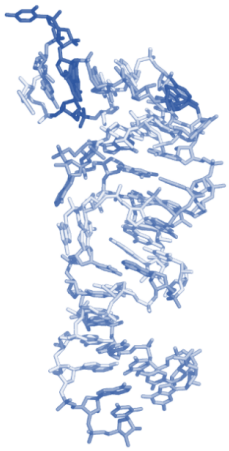

C

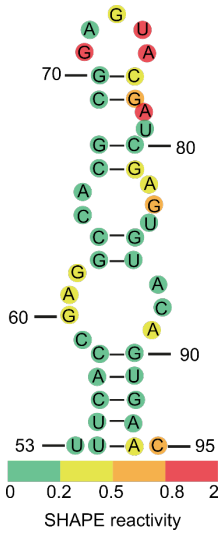

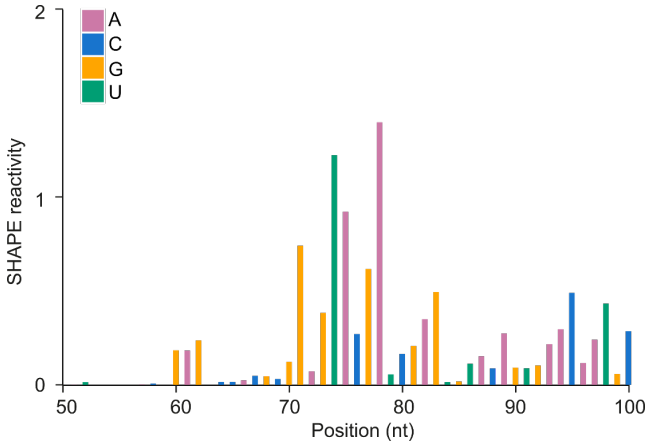

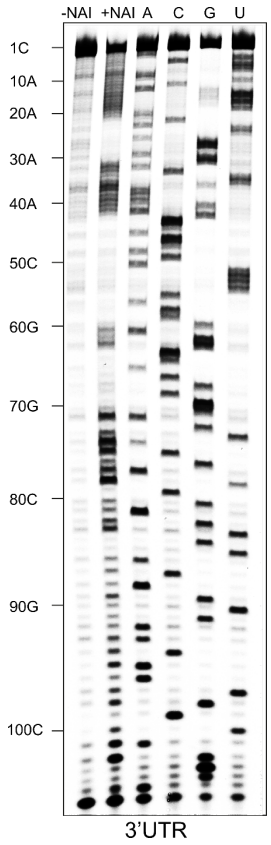

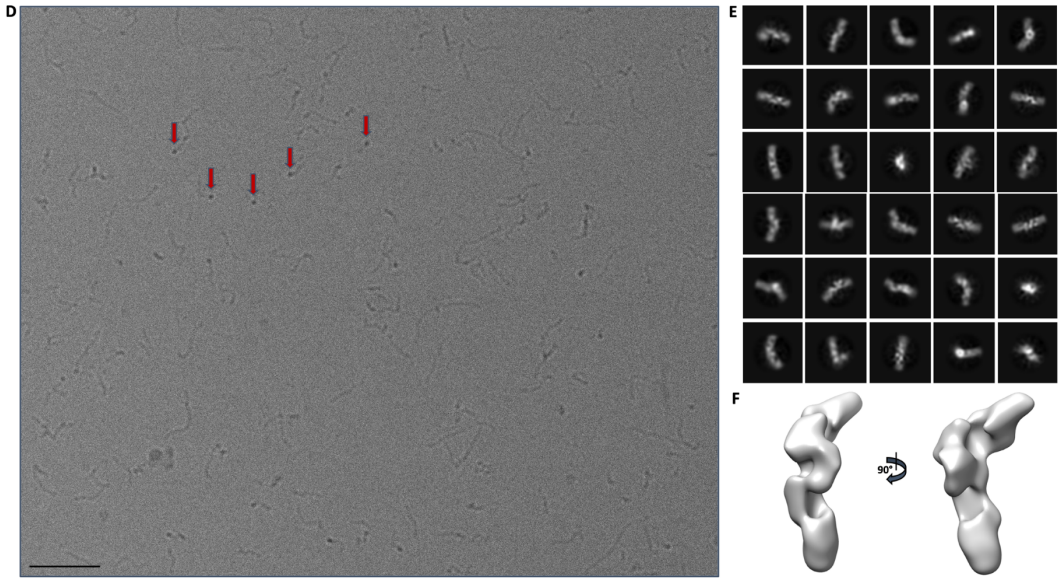

Figure 1. s2m is a conserved structural element in the SARS-CoV-2 genome.
(**A**) Sequence alignment of the s2m element in the 3′ UTRs of SARS-CoV-2 and SARS-CoV. (**B**) The crystal structure of the SARS-CoV s2m element (adapted from Robertson et al., 2005). (**C**) Chemical probing of the 3′ UTR of SARS-CoV-2. RNA was denatured and refolded in the presence of 100 mM K^+ and 0.5 mM Mg^{2+}, then incubated with NAI (+NAI channel) or DMSO control (-NAI channel). NAI modification was detected by reverse transcription stalling and gel-based analysis. Sequencing lanes were generated by adding ddT (for A), ddG (for C), ddC (for G) and ddA (for U) when performing reverse transcription. The lower panel shows quantification of SHAPE signal in the s2m and flanking regions. Calculation was based on the gel in Fig. 1C, by subtracting the signal of the +NAI lane from that of the -NAI lane. The upper panel shows annotation of SHAPE signal on the s2m structure. The bases with SHAPE signal of 0-0.2, 0.2-0.5, 0.5-0.8 and 0.8-2 were coloured with green, yellow, orange and red, respectively. (**D**) Representative cryoEM image of the SARS-CoV-2 3′ UTR at 2.5 µm defocus. The red arrows indicate features that likely correspond to views along the long axis of duplex regions. The black line in the lower left is a 50 nm scalebar. (**E**) The 2D class averages and (**F**) 3D reconstructions as calculated by CryoSparc 2.15.0.

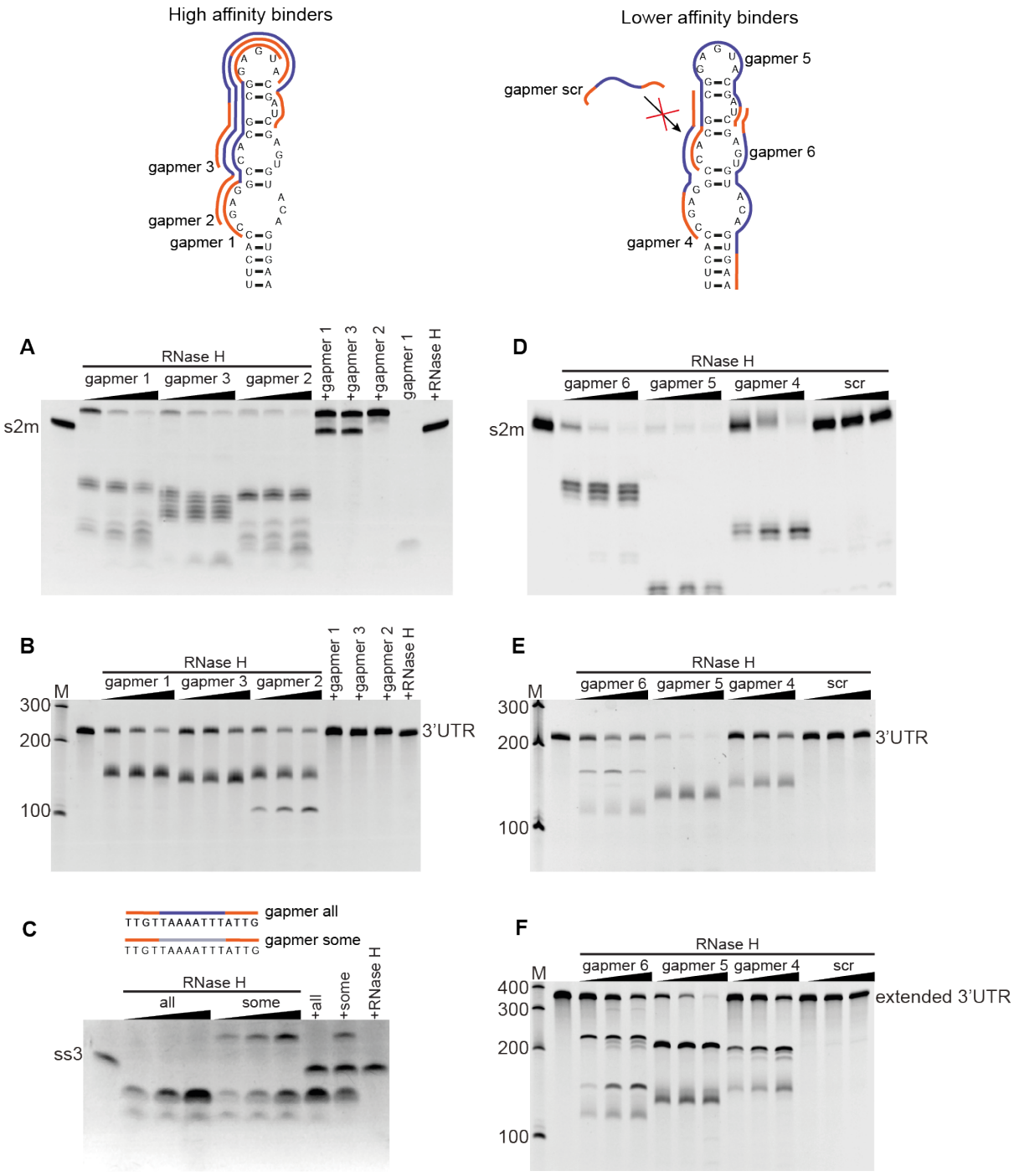

Figure 2. Antisense oligomers direct RNase H cleavage of the s2m element and a conserved single stranded region (ss3) in vitro. The upper panel shows the design of the six gapmers that are complementary to the s2m used in this study, as well as a non-specific control gapmer scr (Table 3). The LNA is indicated in orange and DNA in blue. RNase H cleavage of the isolated s2m (**A, D**), 3′ UTR (**B, E**), the extended 3′ UTR (**F**) and the predicted single-stranded region ss3 (**C**). Three target to gapmer molar ratios were tested: 1:05, 1:1 and 1:2. Incubation of RNA target with RNase H alone does not lead to cleavage (+RNase H, last lane), and is not driven by control gapmers with scrambled DNA sequence (scr). Incubation of RNA

target with gapmer without the addition of RNase H also does not lead to degradation, but does lead to the appearance of a retarded band that likely corresponds to target:gapmer duplex.

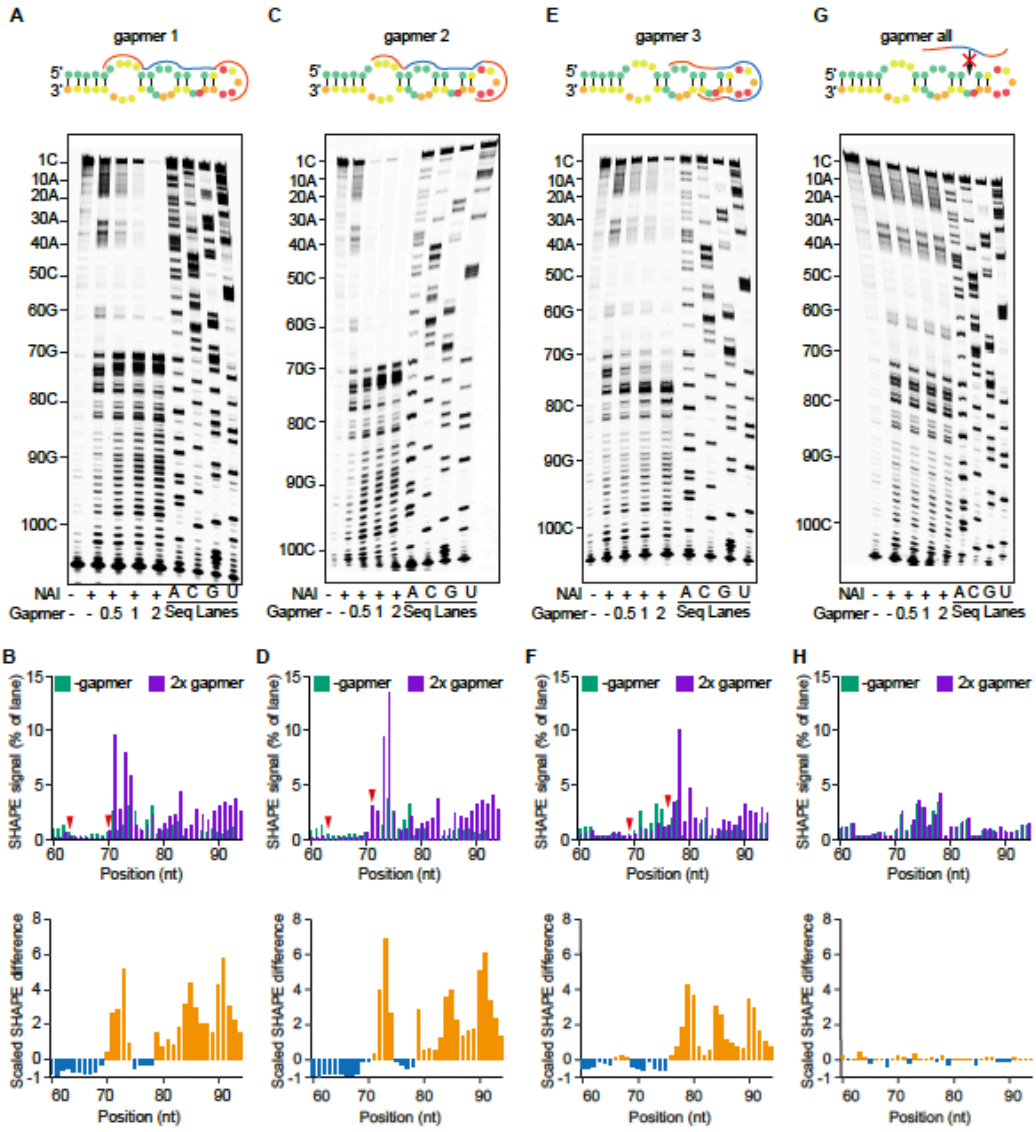

Figure 3. SHAPE probing reveals RNA structure changes induced by LNA gapmers. (**A**, **C**, **E**, **G**) SHAPE probing of SARS-CoV-2 3′ UTR structure in the presence or absence of the gapmer indicated. RNA was denatured and refolded in the presence of 100 mM K^+ and 0.5 mM Mg^{2+}, then incubated with different amounts of gapmer (0×, 0.5×, 1×, 2× that of RNA) and probed using NAI. (**B**, **D**, **F**, **H**) Quantification of A, C, E and G, respectively. Analysis of the differences in SHAPE signal from SARS-CoV-2 3′ UTR alone and in the presence of 2× gapmer. (**A** and **B**) The presence of gapmer 1 induced an increase in SHAPE signal at positions 70-74 and 79-94, highlighted in orange, indicating that these nucleotides are more unstructured. A strong decrease in SHAPE signal was observed at positions 60-69, highlighted in blue, indicating decreased accessibility of these bases, which could be caused by their base-pairing with the gapmer. (**C** and **D**) The reactivity profile in **D** is similar to that in **B**, due to the similar target regions of gapmer 1 and gapmer 2. (**E** and **F**) In the presence of gapmer 3, nucleotides at positions 69-75 are more structured, while nucleotides at positions 76-94 are less structured, as indicated. (**G** and **H**) No significant differences in SHAPE signal could be detected in the presence or absence of the non-specific control gapmer "all", indicating that it is unable to cause structural changes in the SARS-CoV-2 3′ UTR.

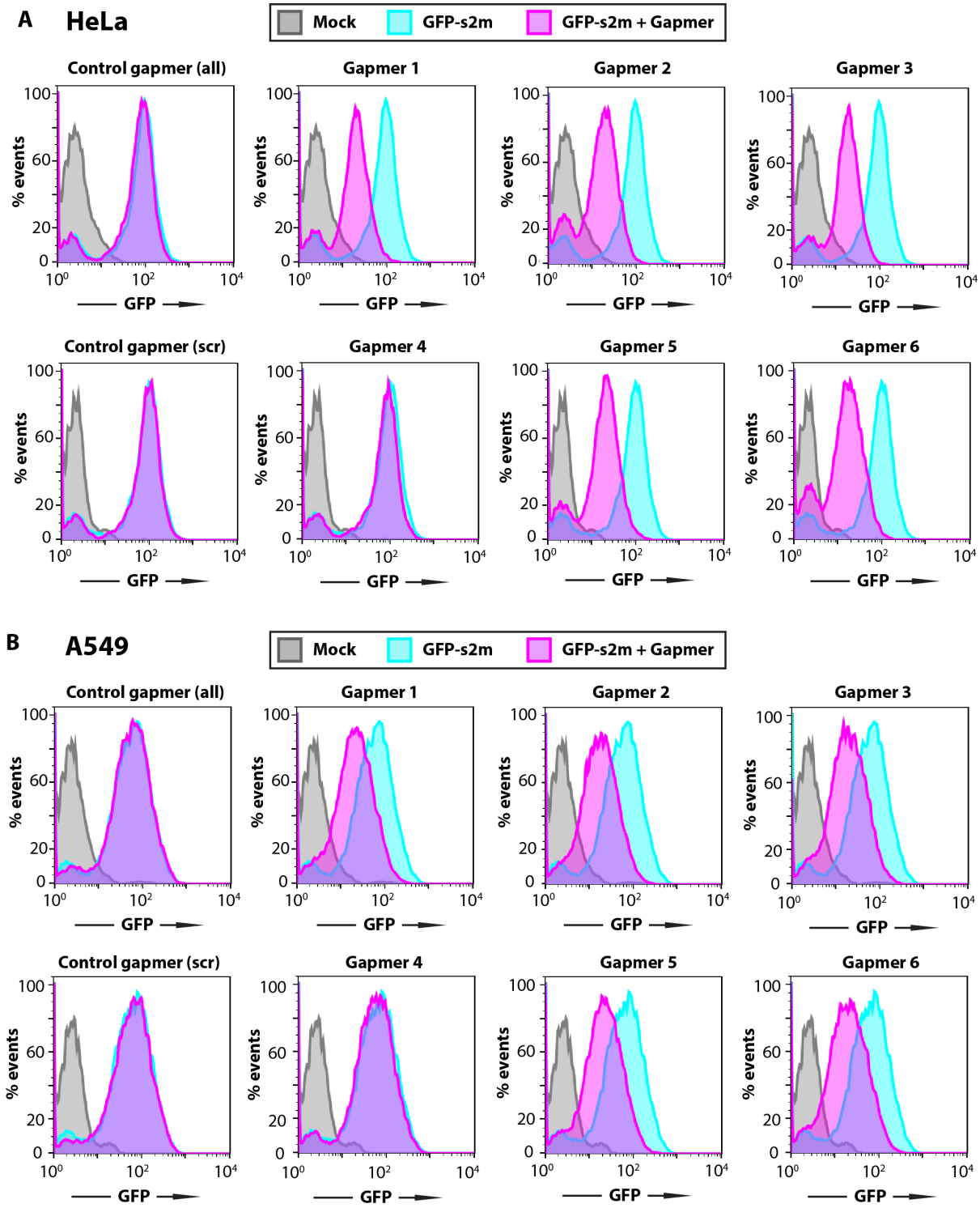

Figure 4. Gapmer-induced reduction of protein levels in cell reporter assays.
Flow cytometry analysis of the GFP expressing cells. HeLa (**A**) and A549 (**B**) cell lines containing a genomic insertion of a GFP reporter construct with the s2m sequence in its 3′ UTR (GFP-s2m) were transfected with 20 nM of the indicated gapmers and analysed 72 h post-transfection by flow cytometry. Treatment with gapmers against the s2m element, but not a nonspecific control gapmer, induced reduction in fluorescence, as detected by flow cytometry. Data are representative of three independent experiments.

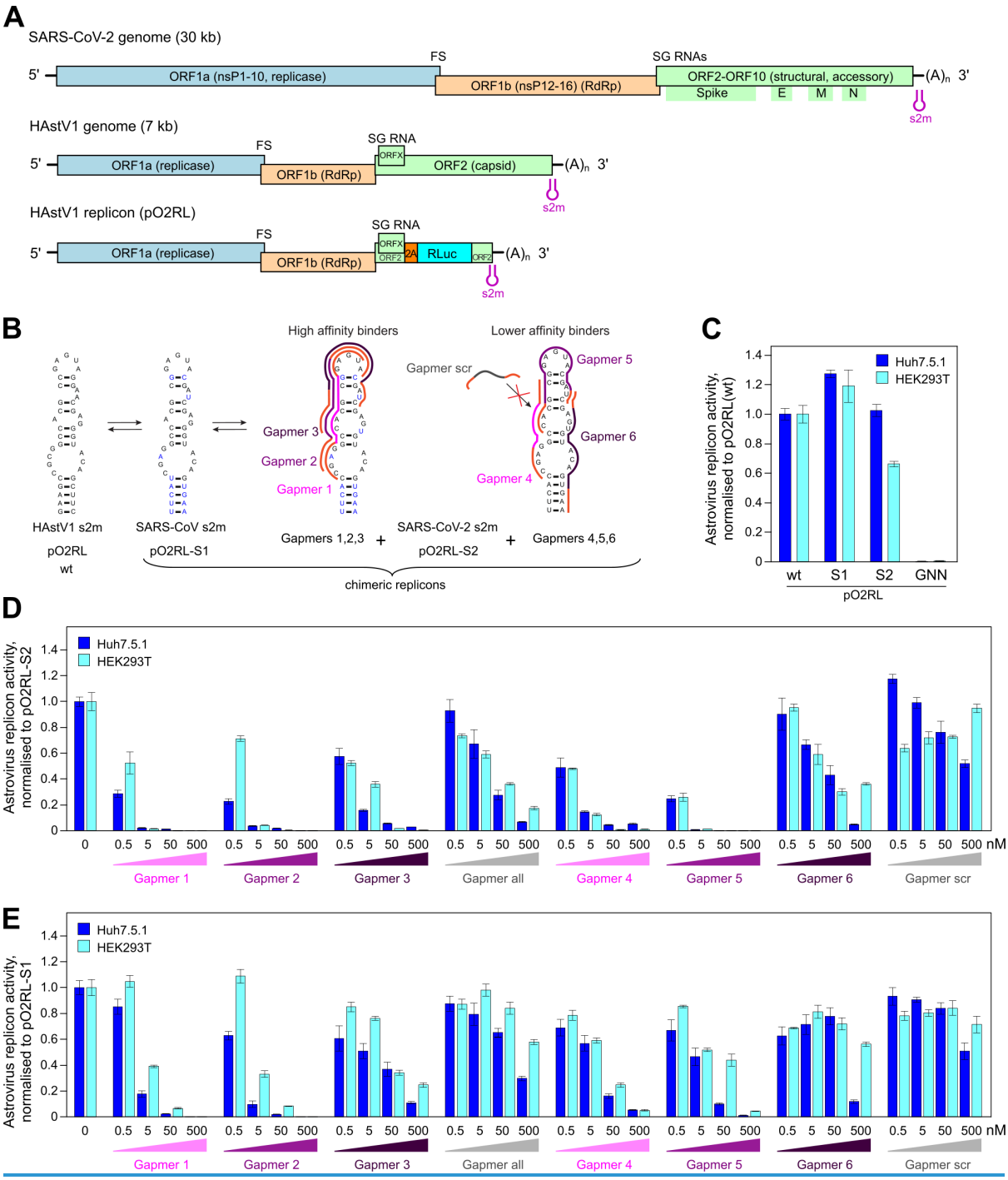

Figure 5. Inhibition of astrovirus replicon activity by gapmers targeting the SARS-CoV-2 s2m RNA element. (**A**) Schematic of the SARS-CoV-2 and human astrovirus 1 (HAstV1) genome organisation. The lower panel represents the astrovirus replicon (pO2RL). FS, frameshift signal; SG, subgenomic; RLuc, Renilla luciferase; RdRp, RNA dependent RNA polymerase. (**B**) Conservation of the s2m 3′ UTR element (two-dimensional representation) between HAstV1, SARS-CoV and SARS-CoV-2. In the astrovirus replicon, the HAstV1 s2m was switched for the SARS-CoV or SARS-CoV-2 s2m; the wild-type and chimeric replicons are indicated below. Gapmers (1, 2, 3 and 4, 5, 6) are colour-coded in light, medium and dark magenta, respectively. (**C**) Luciferase activity of the wildtype, chimeric, and replication-deficient (RdRp GDD motif mutated to GNN) astrovirus replicons measured in Huh7.5.1 (light

blue bars) and HEK293T (dark blue bars) cells. (**D**) Inhibition of the SARS-CoV-2 chimeric replicon by gapmers at 0.5-500 nM concentration range. (**E**) Inhibition of the SARS-CoV chimeric replicon by gapmers at 0.5-500 nM concentration range. For D-E, all data is presented as mean ± s.d.; $n = 3$ biologically independent experiments.

MATERIALS AND METHODS

RNA purification

3′ UTRs and the s2m 47-mer were prepared by in vitro transcription (IVT) using standard protocol. Templates for IVT were generated either by PCR, using Phire Hotstart II polymerase (Thermo Fisher) according to manufacturer's instructions, or by hybridising complementary DNA oligonucleotides (Sigma). Sequences for the PCR primers and the DNA oligonucleotides are given in Table 2. RNA generated by IVT was purified: IVT products were separated on polyacrylamide denaturing gel (National Diagnostics), relevant bands were excised using UV shadowing and electroeluted in TBE (Whatman Elutrap), then cleaned up using PureLinkTM RNA Microscale Kit (Invitrogen). RNA concentrations were estimated using UV absorbance (A260nm) and a calculated extinction coefficient.

Gel-based RNA cleavage assay

Each gapmer was pre-incubated with target RNA in 1× RNase H buffer (Thermo Scientific) for 10 min at 37 °C. 2.5 U of RNase H (Thermo Scientific) was then added and the reaction incubated for 20 min at 37 °C. Reactions were quenched by adding an equal volume of proteinase K mix (0.5 mg/mL enzyme, 100 mM Tris-HCl pH 7.5, 150 mM NaCl, 12.5 mM EDTA, 1% w/v SDS) and incubating at 50 °C for 20 min. RNA was visualised on polyacrylamide 7.5 M urea gel (National Diagnostics) in TBE using SybrGold (Invitrogen).

Chemical probing of the 3' UTR

To probe RNA structure without gapmers, 5 pmol RNA (~350 ng) was dissolved in 9 µl nuclease-free water, and denatured at 95 °C for 90 s, then cooled on ice for 2 min. RNA was refolded by adding 10 µl of 2× SHAPE probing buffer (80 mM HEPES, pH 7.5, 200 mM KCl, 1 mM $MgCl_2$) and incubating at 37 °C for 15 min. 2-methylnicotinic acid imidazolide (NAI) was added to a final concentration of 100 mM in 20 µl reaction; in control reactions, same volume of DMSO was added instead. Reactions were allowed to proceed at 37 °C for 5 min and then quenched by adding 10 µl of 2 M DTT. RNA was purified by loading quenched samples onto Micro Bio-spin Columns with Bio-Gel P-6 (BioRad), followed by ethanol precipitation. Purified RNA was then dissolved in 6 µl water, reverse-transcribed into cDNA and analysed by PAGE as described below.

To probe RNA structure with gapmers, different amounts of gapmers were added to refolded RNA, at molar ratios of 0.5×, 1× or 2×, and incubated at 37 °C for 10 min. The same volume of water was added for the no-gapmer control. After co-incubation, RNA was probed using NAI as described above.

In addition, un-probed input RNA was also subjected to Sanger sequencing: RNA was dissolved in 5 µl water and supplemented with 1 µl of 10 mM corresponding ddNTP (Roche), then reverse-transcribed into cDNA and analysed by PAGE as described below.

Reverse transcription and PAGE analysis of cDNA

6 µl of each RNA-containing sample was mixed with 1 µl of 5 µM Cy5-modified RT primer (sequence given in Table 2) and 0.5 µl of 10 mM dNTPs. The mixture was incubated at 95 °C for 3 min to denature the RNA and then cooled to 50 °C. RT reaction was started by adding 2 µl of 5× RT buffer (100 mM Tris pH 8.3, 500 mM LiCl, 15 mM $MgCl_2$, 5 mM DTT) and 0.5 µl Superscript III enzyme (Invitrogen), mixing quickly with a pipette tip. Reaction was

allowed to proceed at 50 °C for 20 min, then quenched by incubation at 85 °C for 10 min, which inactivates the enzyme. In order to degrade RNA and liberate the complementary cDNA, the reaction mix was then supplemented with 0.5 µl of 2 M NaOH and incubated at 95 °C for 10 min. The reaction was stopped by adding an equal volume of 2× stopping buffer (95% formaldehyde, 20 mM EDTA pH 8.0, 20 mM Tris-HCl pH 7.5, orange G dye) and incubating at 95 °C for 5 min. The resulting cDNA sample was cooled down to 65 °C and analysed on an 8% Acrylamide:Bis-Acrylamide-Urea gel by electrophoresis. The gel was imaged using Typhoon FLA 9000 Gel Imager (GE healthcare).

Quantitative Gel Analysis and SHAPE Reactivity Calculation

Signal intensity of each band on the PAGE gel was detected using ImageQuant TL software and normalized to the total signal of the whole lane. Raw reactivity was generated by subtracting the signal of NAI channel from that of the DMSO control channel; reactivities with negative values were corrected to 0. SHAPE reactivity was generated following the 2/8 % normalization method (Low and Weeks, 2010). To calculate the differences in SHAPE signal in the presence and absence of gapmers, the lanes of NAI channels with 2× gapmer (+gapmer) or without gapmer (-gapmer) were used. The signal intensity of each band was normalized to the total signal of the whole lane. Differences were calculated by subtracting the signal of the +gapmer channel from that of the -gapmer channel and then rescaled to the signal of the -gapmer channel.

Cryo electron microscopy

5 µM purified 3′ UTR in 10 mM Tris pH 7.6, 10 mM KCl, 10 mM NaCl was annealed by sequential incubation at 95 °C for 2 min, at 50 °C for 2 min, at 37 °C for 5 min and then at room temperature. The sample was supplemented with 1 mM $MgCl_2$. 3 µl of the resultant mixture was applied to glow-discharged (EasiGlow Pelco) R2/2 Quantifoil grids (Quantifoil). Excess sample was blotted away with a FEI Vitrobot (IV) (100% humidity, 4 °C, blotting force 0, 3 s blot time) and the grids were vitrified in liquid ethane. The grids were screened with a 200 kV FEI Talos Arctica microscope with a Falcon III camera and a data set was collected on a 300 kV FEI Titan Krios microscope equipped with a Gatan K3 camera. Motion correction, ctf estimation and particle-picking were performed in Warp (Tegunov et al., 2018) and 2D/3D alignments and averaging were carried out with cryoSPARC 2.15 (Punjani et al., 2017).

Gapmer reporter assays.

The s2m sequence or control scrambled sequence of s2m (s2m_scr) was inserted into the 3′ UTR of GFP in H6P plasmid using In-Fusion Cloning kit (TaKaRa) and verified by sequencing. HEK293ET, HeLa and A459 cells, as well as all stable cell lines, were grown in IMDM medium supplemented with 10% FCS at 37 °C in 5% CO_2. All cell lines tested negative for mycoplasma. Constructs in H6P plasmids were used to produce recombinant lentivirus in HEK293ET cells for the stable expression of GFP reporter in mammalian cells from a constitutive SFFV promoter. HeLa and A549 stable cell lines were generated by lentiviral transduction with low MOI (>0.3) to ensure single genomic integrations and were selected for by drug resistance.

To examine the effect of gapmers on GFP expression, HeLa or A549 cells with a stably integrated GFP-s2m/s2m_scr reporter were seeded at 5×10^4 cells per well in 24-well plates. The following day, cells were transfected with 20 nM gapmer using Lipofectamine RNAiMAX (Thermo Fisher Scientific). Flow cytometry analysis was performed 72 h after transfection. Cells were washed twice with warm PBS, detached with trypsin and resuspended in IMDM. All samples were analysed on a BD LSR ii flow cytometer, using the high throughput system

(HTS), and at least 20,000 events were acquired for each sample. Data were analysed in FlowJo (v10.7.1). Main cell population was identified and gated on Forward and Side Scatter using the Auto Gate tool and plotted as a histogram to visualise GFP intensity of cells (measured using B-525 detector).

Virus replicon assays

HEK293T cells (ATCC) were maintained at 37 °C in DMEM supplemented with 10% fetal bovine serum (FBS), 1 mM L-glutamine, and antibiotics. Huh7.5.1 cells (obtained from Apath, Brooklyn, NY; Zhong et al., 2005) were maintained in the same media supplemented with non-essential amino acids. All cells were mycoplasma tested (MycoAlert™ PLUS Assay, Lonza); Huh7.5.1 cells were also tested by deep sequencing.

The HAstV1 replicon system is based on the HAstV1 infectious clone, where the virus genome is left intact up to the end of ORFX, then followed by a foot-and-mouth disease virus 2A sequence and a *Renilla* luciferase (RLuc) sequence fused in the ORF2 reading frame, followed by the last 624 nt of the virus genome and a poly-A tail (Fig. 4A, GenBank accession number MN030571; Lulla and Firth, 2020). The s2m mutations were introduced using site-directed mutagenesis and all constructs were confirmed by sequencing. The resulting plasmids were linearized with *Xho*I prior to T7 RNA transcription.

Huh7.5.1 and HEK293T cells were transfected in triplicate with Lipofectamine 2000 reagent (Invitrogen), using the protocol in which suspended cells are added directly to the RNA complexes in 96-well plates. For each transfection, 100 ng replicon, 10 ng firefly luciferase-encoding purified T7 RNA (RNA Clean and Concentrator, Zymo research), the indicated amount of gapmers, and 0.3 µl Lipofectamine 2000 in 20 µl Opti-Mem (Gibco) supplemented with RNaseOUT (Invitrogen; diluted 1:1,000 in Opti-Mem) were added to each well containing 5×10^4 cells in 100 µl DMEM supplemented with 5% FBS, and incubated at 37 °C for 12 h (Huh7.5.1) or 18 h (HEK293T). Firefly and Renilla luciferase activities were determined using the Dual Luciferase Stop & Glo Reporter Assay System (Promega). Replicon activity was calculated as the ratio of Renilla (subgenomic reporter) to Firefly (cap-dependent translation, loading control), normalized by the same ratio for the control replicon, as indicated for each experiment. Three independent experiments, each in triplicate, were performed to confirm reproducibility of results.

Cytotoxicity assay

The analysis of cellular cytotoxicity was performed using the CyQUANT LDH cytotoxicity assay (Thermo Scientific). Leaked cytoplasmic enzyme LDH in cell culture supernatants was quantified after enzymatic conversion, and absorbance was measured at 490 nm in a 96-well plate reader according to the manufacturer's instructions.

TABLES

Table 1. Sequence of the RNA used in this study

SARS-CoV-2 s2m sequence used in RNase H assays *in vitro* and in GFP reporter assays (47 nt) GGAGUUCACCGAGGCCACGCGGAGUACGAUCGAGUGUACAGUGAAUU
Scrambled control sequence used in GFP reporter assays (47 nt) AGCCGGGCUGGAAGAUACUGCCCAAAUAGGGAACUUUGACGCGGUUG
SARS-CoV-2 3′ UTR (220 nt) UAGCAAUCUUUAAUCAGUGUGUAACAUUAGGGAGGACUUGAAAGAGCCACCACAUUUUCAC CGAGGCCACGCGGAGUACGAUCGAGUGUACAGUGAACAAUGCUAGGGAGAGCUGCCUAUAU GGAAGAGCCCUAAUGUGUAAAAUUAAUUUUAGUAGUGCUAUCCCCAUGUGAUUUUAAUAGC UUCUUAGGAGAAUGACAAAAAAAAAAAAAAAAAAAAA
SARS-CoV-2 extended 3′ UTR (358 nt) ACUCAUGCAGACCACACAAGGCAGAUGGGCUAUAUAAACGUUUUCGCUUUUCCGUUUACGAU AUAUAGUCUACUCUUGUGCAGAAUGAAUUCUCGUAACUACAUAGCACAAGUAGAUGUAGUU AACUUUAAUCUCACAUAGCAAUCUUUAAUCAGUGUGUAACAUUAGGGAGGACUUGAAAGAG CCACCACAUUUUCACCGAGGCCACGCGGAGUACGAUCGAGUGUACAGUGAACAAUGCUAGGG AGAGCUGCCUAUAUGGAAGAGCCCUAAUGUGUAAAAUUAAUUUUAGUAGUGCUAUCCCCAU GUGAUUUUAAUAGCUUCUUAGGAGAAUGACAAAAAAAAAAAAAAAAAAAAA
SARS-CoV-2 ss3 (16 nt). A conserved region predicted to be single-stranded in the genome; positions 1359-1374 relative to the NC_045512.2 reference (Rangan et al., 2020) UUGUUAAAAUUUAUUG

Table 2. Primers for IVT and SHAPE analysis

Name	Type	Sequence
3′ UTR_F	IVT primer	GTTTTTTAATACGACTCACTATAGCAATCTTTAATCAGTGTG TAACATTAGG
Extended 3′ UTR_F	IVT primer	GTTTTTTAATACGACTCACTATTACTCATGCAGACCACACA AGGC
3′ UTR_R	IVT primer	TTTTTTTTTTTTTTTTTTTTTGTCATTCTCCTAAGAAGC
S2M_F	IVT primer	GTTTTTTAATACGACTCACTATAGGAGTTCACCGAGGCCAC GCGGAGTACGATCGAGTGTACAGTGAATT
S2M_R	IVT primer	AATTCACTGTACACTCGATCGTACTCCGCGTGGCCTCGGTG AACTCCTATAGTGAGTCGTATTAAAAAAC
COV19_RT1	SHAPE Primer	Cy5-TTTTGTCATTCTCCTAAGAAGCT
COV19_RT2	SHAPE Primer	Cy5-CTCTTCCATATAGGCAGCTC

Table 3 Gapmers used in this study

Notation: * = phosphorothioate backbone linkage; [+X] = LNA base X.
Melting temperature predictions were obtained using an online oligo design tool (https://www.qiagen.com/).

Name	Sequence	DNA T_m (°C)	RNA T_m (°C)
Gapmer 1	[+A]*[+C]*[+T]*[+C]*C*G*C*G*T*G*G*C*[+C]*[+T]*[+C]*[+G]	85	93
Gapmer 2	[+T]*[+A]*[+C]*[+T]*C*C*G*C*G*T*G*G*[+C]*[+C]*[+T]*[+C]	81	97
Gapmer 3	[+G]*[+A]*[+T]*[+C]*G*T*A*C*T*C*C*G*[+C]*[+G]*[+T]*[+G]	78	88
Gapmer 4	[+G]*[+C]*G*T*G*G*C*C*[+T]*[+C]*[+G]	69	76
Gapmer 5	[+G]*[+A]*T*C*G*T*A*C*T*C*C*G*C*[+G]*[+T]*[+G]	70	76
Gapmer 6	[+T]*[+T]*[+C]*A*C*T*G*T*A*C*A*C*T*[+C]*[+G]*[+A]	68	79
scr	[+A]*[+C]*C*G*T*G*C*G*G*T*A*T*T*[+C]*[+G]*[+C]	71	75
all	[+C]*[+A]*[+A]*[+T]*A*A*A*T*T*T*T*A*[+A]*[+C]*[+A]*[+A]	53	50
some	[+C]*[+A]*[+A]*[+T]AAATTTTA[+A]*[+C]*[+A]*[+A]	53	50

SUPPLEMENTARY FIGURES

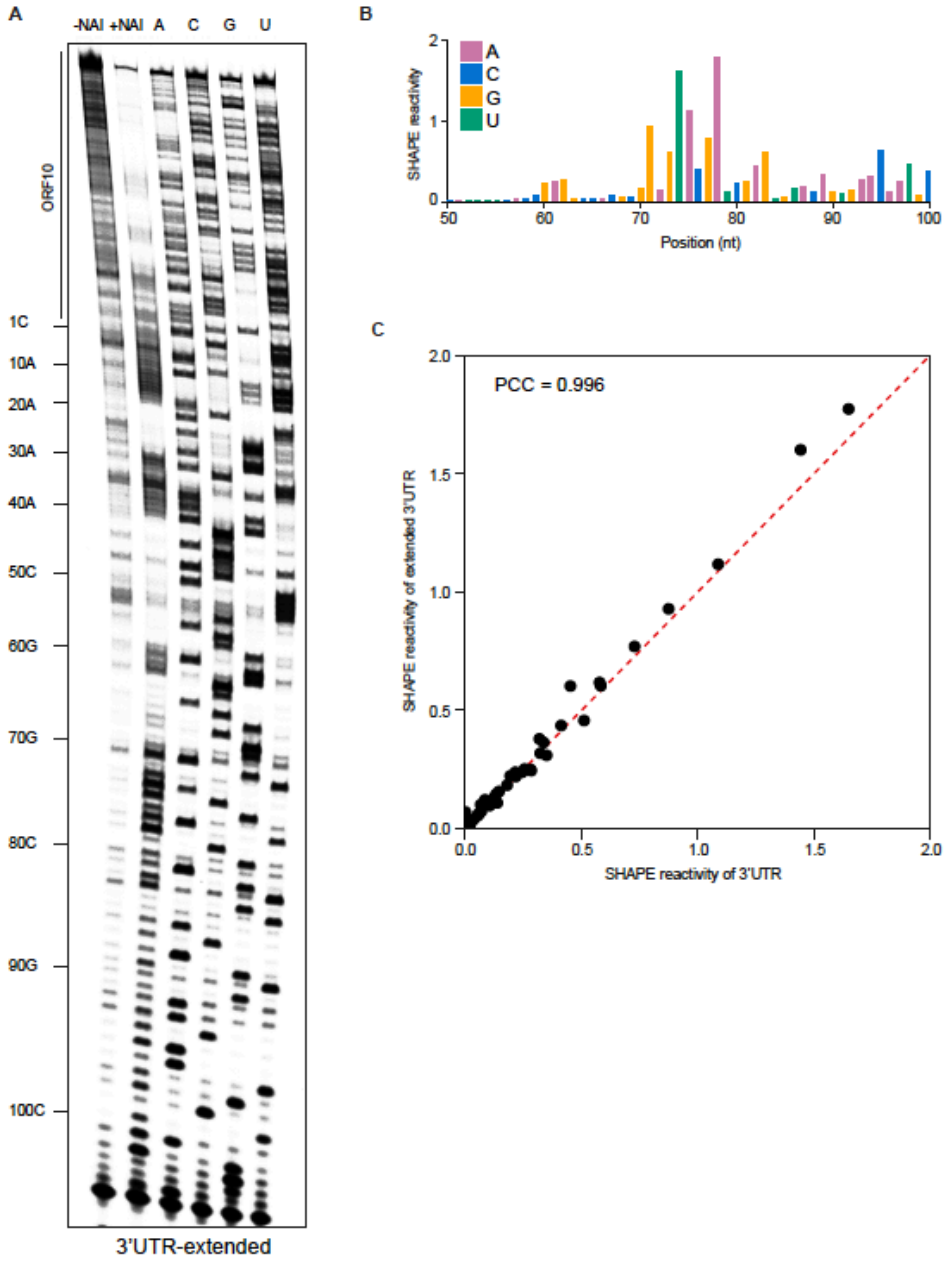

Figure S1, related to Figure 1. **SHAPE analysis of the extended 3′ UTR of SARS-CoV-2** (**A**) Chemical probing of the extended 3′ UTR of SARS-CoV-2 (including ORF10 and the region immediately upstream of it). RNA was denatured and refolded in the presence of 100 mM K^+ and 0.5 mM Mg^{2+}, then incubated with NAI (+NAI channel) or DMSO control (-NAI channel). NAI modification was detected by reverse transcription stalling and gel-based analysis. Sequencing lanes were generated by adding ddT (for A), ddG (for C), ddC (for G) and ddA (for U) when performing reverse transcription. (**B**) Quantification of SHAPE signal on at the s2m element and flanking regions. Calculation was based on the gel in Fig. S1A, by subtracting the signal of the +NAI lane from that of the -NAI lane. (**C**) Agreement of SHAPE signal on s2m structure in the 3′ UTR and the extended 3′ UTR of SARS-CoV-2. Pearson correlation coefficient was calculated based on the SHAPE signals shown in Fig. 1C and Fig. S1B.

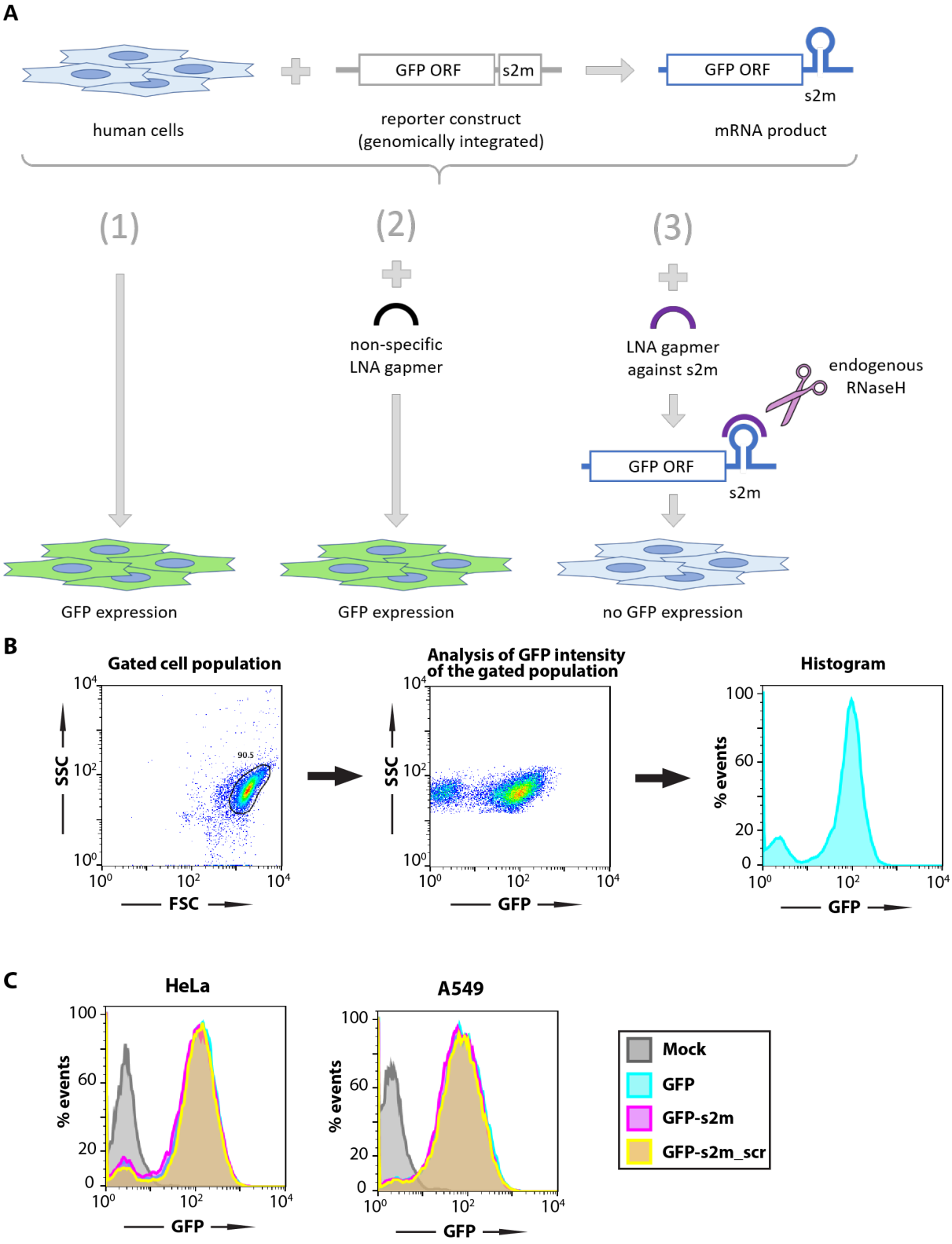

Figure S2, related to Figure 4. **s2m element does not influence RNA translation in the reporter assay in human cells.** (**A**) Schematic of the GFP reporter assay. (**B**) Gating and data visualisation strategy of the reporter assay data. Main cell population was identified and gated on Forward and Side Scatter using the Auto Gate tool and plotted as a histogram to visualise GFP intensity of cells. (**C**) HeLa and A549 cell lines containing a genomic insertion of a GFP reporter construct without additional insertion in its 3′ UTR (GFP), with the s2m sequence in

its 3′ UTR (GFP-s2m) or with a scrambled sequence insertion in its 3′ UTR (GFP-s2m_scr) were analysed by flow cytometry. Data are representative of two independent experiments.

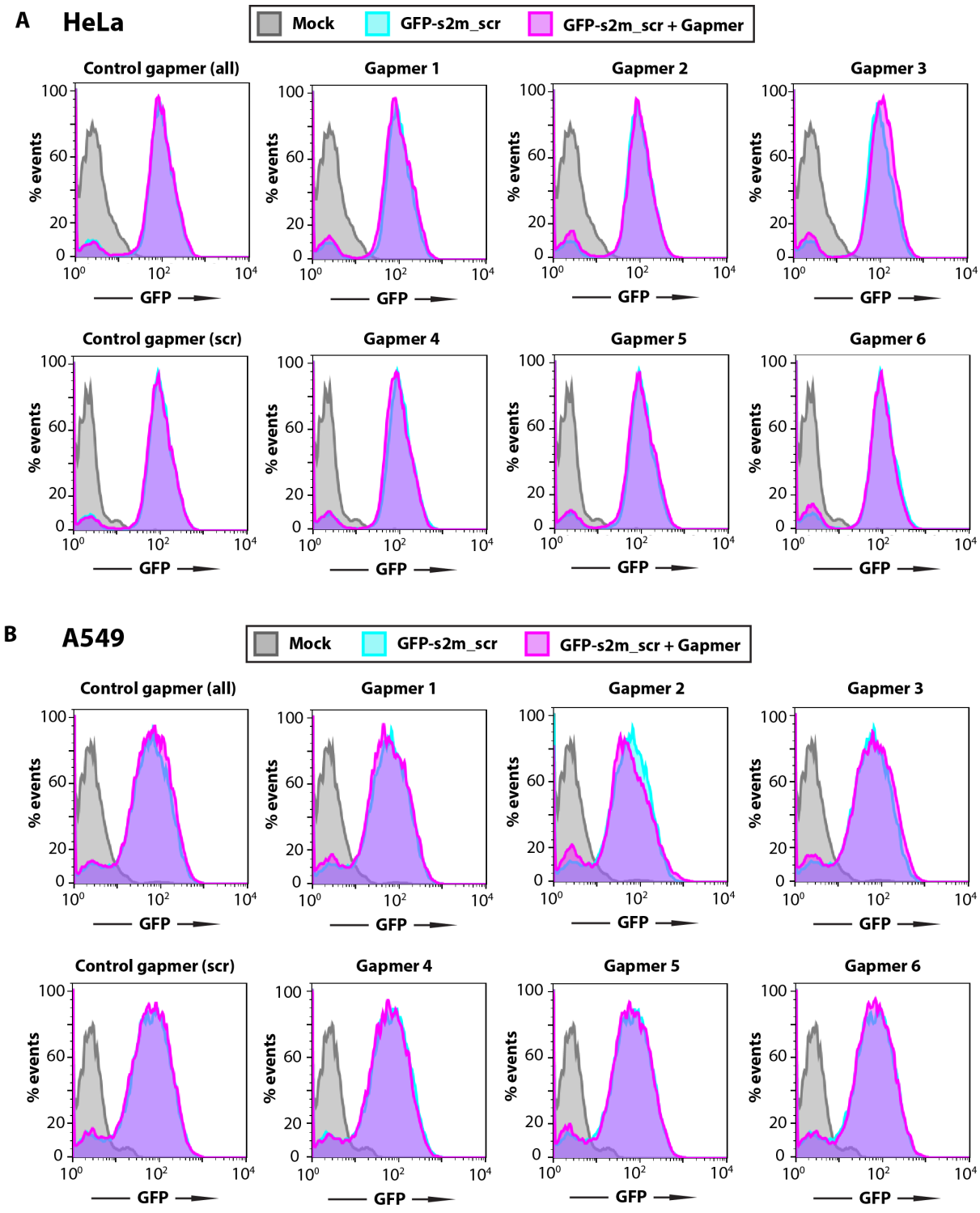

Figure S3, related to Figure 4. **Gapmer silencing effect relies of sequence-specific gapmer-target interaction.** HeLa (**A**) and A549 (**B**) cell lines containing a control genomic insertion of a GFP reporter construct with a scrambled sequence inserted in its 3′ UTR (GFP-s2m_scr) were transfected with 20 nM of the indicated gapmers and analysed 72 h post-transfection by flow cytometry. The control cell lines containing GFP reporter with a scrambled sequence insertion in the 3′ UTR show no appreciable change in fluorescence upon treatment with the gapmers targeted against the s2m element. Data are representative of three independent experiments.

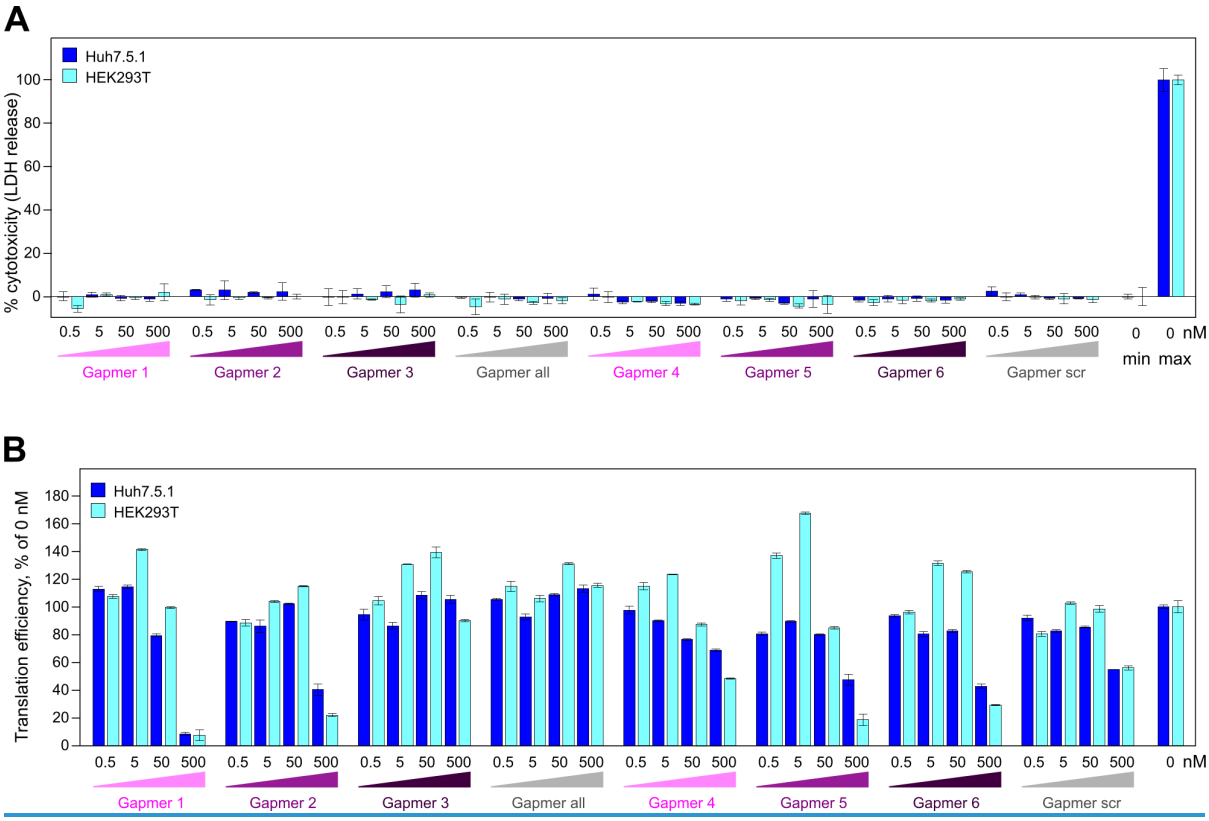

Figure S4, related to Figure 5. **Testing the cytotoxic and off-target effects of gapmers.** (**A**) Toxicity assay for gapmer-treated cells. Cells were treated with 0.5-500 nM gapmers for 24 h. Supernatant was used to measure cell viability, calculated as the ratio of released to total lactate dehydrogenase (LDH) activity; "max" = maximum LDH measured for fully lysed cells. (**B**) The effect on translation measured as a readout of capped T7 RNA encoding firefly luciferase at 0.5-500 nM gapmer concentration, normalized to untreated cells. All data is presented as mean ± s.d.; $n = 3$ biologically independent experiments.